Spallation cross sections for ^{nat}Fe and ^{nat}Cu targets for 120 GeV/c protons and pions

A. Ferrari,[1] F. P. La Torre,[1,2] G. P. Manessi,[1,3,*] F. Pozzi,[1,4] and M. Silari[1]
[1]*CERN, 1211 Geneva 23, Switzerland*
[2]*University of Bern, AEC-LHEP, Sidlerstrasse 5, 3102 Bern, Switzerland*
[3]*Department of Physics, University of Liverpool, L69 7ZE Liverpool, United Kingdom*
[4]*Lehrstuhl für Nukleartechnik, Technische Universität München, Boltzmannstrasse 15, 85748 Garching, Germany*
(Received 27 January 2014; published 14 March 2014)

Spallation cross sections from thin natural copper and iron targets bombarded by a mixed 120 GeV/c proton/pion beam were measured in an activation experiment at CERN. The beam intensity was monitored by a calibrated ionization chamber and the activity of several spallation products was measured (14 for copper and 16 for iron) by γ spectrometry, allowing the absolute cross section of the mixed hadron beam to be derived. Monte Carlo simulations with the FLUKA code provided the ratio between the proton- and pion-induced reaction cross sections for a given spallation product, allowing us to extrapolate the individual cross sections for the proton- and the pion-induced reactions. Where possible the values were compared with literature data and showed to be generally in agreement with the highest energy data available.

DOI: 10.1103/PhysRevC.89.034612 PACS number(s): 25.40.Sc, 25.80.−e

I. INTRODUCTION

Spallation refers to nuclear inelastic reactions that occur when subatomic particles with incident energy higher than 100–150 MeV interact with a target nucleus. At these energies the de Broglie wavelength is short enough to allow the particle to interact with the individual nucleons inside the nucleus. The incident particle first undergoes a series of reactions with the nucleons, where high-energy secondary particles (such as protons, neutrons, and pions) from a few MeV up to the energy of the incident particle are created inside the nucleus (intranuclear cascade). Some of these high-energy hadrons, together with low-energy particles in the MeV range, leave the nucleus and may induce other spallation reactions in a different nucleus (internuclear cascade). This process mainly occurs in thick targets. The nucleus, which is in an excited state, relaxes by emitting low-energy particles, mostly neutrons. After evaporation the final nucleus (spallation product) may be radioactive and decay by γ emission [1]. An accurate knowledge of the spallation product inventory within a target is important for many applications: disposal of material, operation, maintenance, safety and decay heat analysis for neutron spallation sources [2], activation issues in high-energy particle accelerators [3], and benchmarking of Monte Carlo codes [4]. The knowledge of the reaction cross section for a spallation product is therefore fundamental. Spallation cross section data are widely available for energies up a few GeV [5], but for higher energies (especially above 28 GeV) very limited data have been published. This is particularly true for pion-induced reactions for which, to the best of our knowledge, no data are available. The aim of this paper is to provide proton- and pion-induced spallation cross sections at 120 GeV/c for the production of 14 radioisotopes in ^{nat}Cu and 16 radioisotopes in ^{nat}Fe targets. These have been derived from activation experiments carried out with a 120 GeV/c mixed proton/pion beam at the CERN-EU high-energy Reference Field (CERF) facility [6] at CERN. These spallation reactions are of direct relevance in activation studies, since ^{nat}Cu and ^{nat}Fe are commonly employed in high-energy particle accelerators and their surrounding structures.

II. MATERIALS AND METHODS

A. Experimental setup

The experiments were performed by exposing hyperpure ^{nat}Cu and ^{nat}Fe foils to the primary beam at the CERF facility, which is installed in one of the secondary beam lines (H6) from the Super Proton Synchrotron (SPS) in the North Experimental Area on the Prévessin site of CERN. The incoming hadron beam is composed by 61% positive pions, 35% protons, and 4% positive kaons [7] with momentum of 120 GeV/c. For simplicity we assume that the particle energy is 120 GeV, even if the actual value is slightly lower. For the calculations the kaon fraction has been redistributed on the other two components according to their relative weight, i.e., the beam composition has been assumed to be 63.5% positive pions and 36.5% protons. This redistribution has a negligible effect because of the limited importance of the kaon component, whose relative weight is well below the final relative uncertainty on the cross-section values derived from the experiment, and because the kaon-induced spallation cross section lies in between the proton- and the pion-induced one as verified via FLUKA [8,9] Monte Carlo simulations. The beam is delivered to CERF with a typical intensity in the range 10^6 to 10^8 particles per SPS spill, with a beam extraction time of about 10 s over an SPS cycle of about 45 s.

The ^{nat}Cu and ^{nat}Fe foils with dimensions 50 × 50 mm^2 were fixed on a plexiglass frame mounted on both ends of a hollow aluminum tube placed downstream of an ionization chamber (IC) used as beam monitor (see Fig. 1). The foils were irradiated in sandwiches of three to take into account the recoil of some of the nuclei produced in the spallation process that can leave the foil in the same direction of the primary

*giacomo.manessi@cern.ch

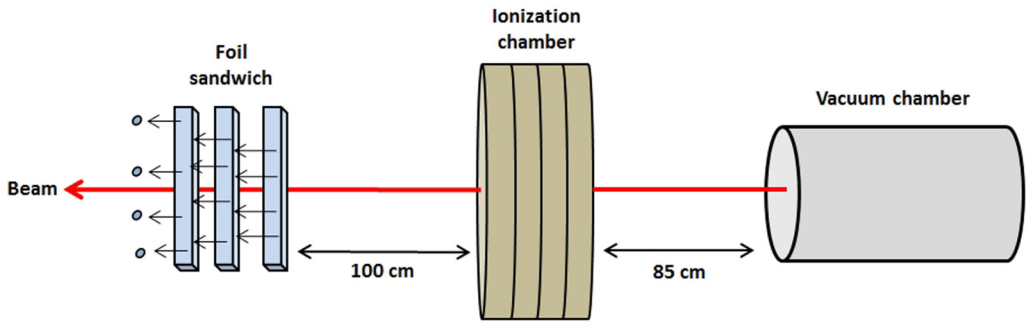

FIG. 1. (Color online) Experimental setup (not to scale).

beam (due to the so-called Lorentz boost [1]). To maintain the equilibrium between the loss of recoil nuclei knocked out of the foil and the gain of nuclei knocked into the foil from upstream material, only the central one must be considered for data analysis, whereas the upstream and the downstream ones act as catchers. These catchers, having the same thickness of the central foil, are thick enough to capture all the knocked on or knocked back products. The beam size was smaller than the foil dimensions so that all particles traversing the IC hit the foils. To evaluate the contribution of scattered radiation to the foil activation an additional foil was exposed out of beam.

The foil thicknesses were 0.5 mm, 0.25 mm, and 0.125 mm for ^{nat}Cu; 2 mm for ^{nat}Fe, with 1% estimated uncertainty. The thicknesses were chosen as a compromise between the need of an induced activity high enough to reduce the statistical uncertainty of the γ-spectrometry measurements and the need of thin targets, i.e., targets in which the energy lost by the incident beam is small ($E_{loss}/E_{beam} \leqslant 5\%$ [1]). This reduces to a minimum the production of secondary particles inside the target, which generally undergo further collisions and could result in internuclear cascades. By assuming that the value of the interaction lengths for protons and pions at 120 GeV is similar to the one at 18 GeV (i.e., 140.2 $\pm$ 3.2 g/cm^2 for protons, 163.8 $\pm$ 9.0 g/cm^2 for pions [10]), the beam fraction that interacts in the target is always less than 1%. This guarantees that, even though the average fraction of energy of the incident beam lost in the target cannot be precisely estimated, the overall influence of the target on the beam transmission is negligible.

B. Theory

The cross section of the reaction $A(p,x)B$ or $A(\pi^+,x)B$, where A is ^{nat}Cu or ^{nat}Fe, B is the radioisotope produced in the foil by the spallation reaction, and x is the reaction product escaping the foil, was measured via the well-established foil activation technique (see, e.g., [11] and references therein quoted). If $A(t)$ (Bq) is the activity of the radioisotope B, λ is its decay constant (s^{-1}), t_{IRR} and $t_{WAIT}(s)$ are the irradiation time and waiting time (i.e., the time elapsed from the end of the irradiation until the foil is counted), N_x is the foil surface atomic density (cm^{-2}), ϕ' is the particle flux (number of particles per second traversing the foil), the production cross section σ of the radioisotope B can be obtained as [11]:

$$\sigma = \frac{A(t)}{N_x \phi'(1 - e^{-\lambda \cdot t_{IRR}}) e^{-\lambda \cdot t_{WAIT}}}. \quad (1)$$

$A(t)$ is measured by γ spectrometry, while t_{WAIT} and t_{IRR} must be recorded. In the present experiment t_{WAIT} was recorded manually while t_{IRR} was obtained from the log file of the acquisition system. The cross section σ is the beam effective cross section, i.e., averaged over the pion and proton components: $\sigma = 0.635\sigma_\pi + 0.365\sigma_p$, where σ_p and σ_π are the proton- and pion-induced spallation cross sections. Their values can be derived if one knows the ratio σ_p/σ_π. This ratio can be obtained from FLUKA simulations. Although FLUKA cannot compute the absolute cross-section value at very high energies with the required accuracy, it is reliable in determining the cross-section ratio of a reaction induced by different particles at the same energy. The ratio can be obtained by running the nuclear interaction models of FLUKA in interaction-only mode, accounting for both absorption and quasielastic reactions [11]. The output file provides the cross section for each isotope produced in the interaction between the primary and the target. By running two simulations (for protons and for pions) one obtains the ratio σ_p/σ_π for the reaction of interest. The cross sections for protons and pions

TABLE I. Foil atomic surface densities.

Fe foils ($\rho_{Fe} = 7.874$ g/cm^3, $M_{Fe} = 55.840$ g/mol)			
Foil thickness X_{Fe}	2.0 mm		
N_x	1.6983×10^{22} cm^2		
Cu foils ($\rho_{Cu} = 8.920$ g/cm^3, $M_{Cu} = 63.546$ g/mol)			
Foil thickness X_{Cu}	0.125 mm	0.250 mm	0.500 mm
N_x	1.0567×10^{21} cm^2	2.1133×10^{21} cm^2	4.2266×10^{21} cm^2

TABLE II. Cross sections of the spallation reactions on ^{nat}Cu derived from the activation experiment.

^{nat}Cu$(p,x)^{41}$Ar	0.62 ± 0.11 mb	^{nat}Cu$(\pi^+,x)^{41}$Ar	0.43 ± 0.08 mb
^{nat}Cu$(p,x)^{42}$K	2.23 ± 0.40 mb	^{nat}Cu$(\pi^+,x)^{42}$K	1.69 ± 0.30 mb
^{nat}Cu$(p,x)^{43}$K	0.93 ± 0.19 mb	^{nat}Cu$(\pi^+,x)^{43}$K	0.66 ± 0.14 mb
^{nat}Cu$(p,x)^{43}$Sc	2.73 ± 0.26 mb	^{nat}Cu$(\pi^+,x)^{43}$Sc	2.62 ± 0.25 mb
^{nat}Cu$(p,x)^{44}$Sc	3.80 ± 0.17 mb	^{nat}Cu$(\pi^+,x)^{44}$Sc	3.46 ± 0.15 mb
^{nat}Cu$(p,x)^{47}$Sc	1.85 ± 0.22 mb	^{nat}Cu$(\pi^+,x)^{47}$Sc	1.42 ± 0.17 mb
^{nat}Cu$(p,x)^{48}$Cr	0.21 ± 0.06 mb	^{nat}Cu$(\pi^+,x)^{48}$Cr	0.21 ± 0.06 mb
^{nat}Cu$(p,x)^{48}$Sc	1.16 ± 0.21 mb	^{nat}Cu$(\pi^+,x)^{48}$Sc	0.83 ± 0.15 mb
^{nat}Cu$(p,x)^{52}$Mn	3.83 ± 0.52 mb	^{nat}Cu$(\pi^+,x)^{52}$Mn	3.87 ± 0.52 mb
^{nat}Cu$(p,x)^{55}$Co	0.51 ± 0.10 mb	^{nat}Cu$(\pi^+,x)^{55}$Co	0.56 ± 0.11 mb
^{nat}Cu$(p,x)^{56}$Mn	2.68 ± 0.14 mb	^{nat}Cu$(\pi^+,x)^{56}$Mn	2.01 ± 0.10 mb
^{nat}Cu$(p,x)^{57}$Ni	0.77 ± 0.14 mb	^{nat}Cu$(\pi^+,x)^{57}$Ni	0.77 ± 0.14 mb
^{nat}Cu$(p,x)^{58}$Co	18.82 ± 6.01 mb	^{nat}Cu$(\pi^+,x)^{58}$Co	18.07 ± 5.77 mb
^{nat}Cu$(p,x)^{61}$Cu	11.12 ± 0.51 mb	^{nat}Cu$(\pi^+,x)^{61}$Cu	11.46 ± 0.52 mb

can then be easily derived:

$$\sigma_\pi = \frac{\sigma}{0.635 + 0.365\frac{\sigma_p}{\sigma_\pi}} \quad \text{and} \tag{2}$$

$$\sigma_p = \frac{\sigma - 0.635\sigma_\pi}{0.365}. \tag{3}$$

C. Parameters

The hyperpure ^{nat}Cu and ^{nat}Fe foils have the following compositions, as declared by the manufacturer [12]: 99.991% ^{nat}Cu, with impurities in ppm: Ag 70, Fe 2, Ni 2, Pb2, Si 2, Al 1, Bi 1, Ca 1, Mg1, Sn 1, Mn <1, Na <1, Cr <1; 99.998% ^{nat}Fe, impurities in ppm: Ag 1, Al 2, Ca 3, Cr 1, Cu 2, Mg 2, Mn 1, Ni1, Si 3. The effect of the impurities on the radioisotope production is negligible. This has been verified via several sets of FLUKA simulations, in which the foils were first simulated as 100% pure, and then with added impurities. The values of the surface atomic densities N_x to be used in expression (1) are obtained from the foil density, the molar mass, and the thickness (see Table I).

The beam monitoring was provided by an air-filled, parallel-plate, transmission-type IC, calibrated with the foil activation technique using the ^{27}Al$(p,3pn)^{24}$Na and ^{nat}Cu$(p,x)^{24}$Na monitor reactions [11]. The beam intensity recorded by the IC was written every second in a log file, from which the value of ϕ' to be used in expression (1) was obtained. Since the beam intensity was recorded every second, the irradiation time was subdivided in one second irradiation slots ($t_{IRR} = 1s$). For each of these slots a corresponding waiting time t_{WAIT} was considered. Thanks to this method any fluctuation in the beam intensity during the irradiation was properly taken into account.

The foils were counted in the CERN γ-spectrometry laboratory with a Canberra low background coaxial high-purity germanium (HPGe) detector. For a more accurate analysis of

TABLE III. Cross sections of the spallation reactions on ^{nat}Fe derived from the activation experiment.

^{nat}Fe$(p,x)^{24}$Na	4.02 ± 0.45 mb	^{nat}Fe$(\pi^+,x)^{24}$Na	2.96 ± 0.33 mb
^{nat}Fe$(p,x)^{41}$Ar	0.84 ± 0.16 mb	^{nat}Fe$(\pi^+,x)^{41}$Ar	0.53 ± 0.10 mb
^{nat}Fe$(p,x)^{42}$K	4.28 ± 0.57 mb	^{nat}Fe$(\pi^+,x)^{42}$K	3.18 ± 0.43 mb
^{nat}Fe$(p,x)^{43}$K	1.42 ± 0.19 mb	^{nat}Fe$(\pi^+,x)^{43}$K	0.92 ± 0.12 mb
^{nat}Fe$(p,x)^{43}$Sc	3.72 ± 0.63 mb	^{nat}Fe$(\pi^+,x)^{43}$Sc	3.73 ± 0.63 mb
^{nat}Fe$(p,x)^{44}$Sc	8.32 ± 0.93 mb	^{nat}Fe$(\pi^+,x)^{44}$Sc	7.87 ± 0.88 mb
^{nat}Fe$(p,x)^{46}$Sc	6.07 ± 2.36 mb	^{nat}Fe$(\pi^+,x)^{46}$Sc	4.87 ± 1.89 mb
^{nat}Fe$(p,x)^{47}$Sc	3.96 ± 0.54 mb	^{nat}Fe$(\pi^+,x)^{47}$Sc	2.93 ± 0.40 mb
^{nat}Fe$(p,x)^{48}$Cr	0.59 ± 0.08 mb	^{nat}Fe$(\pi^+,x)^{48}$Cr	0.64 ± 0.08 mb
^{nat}Fe$(p,x)^{48}$Sc	0.61 ± 0.13 mb	^{nat}Fe$(\pi^+,x)^{48}$Sc	0.37 ± 0.08 mb
^{nat}Fe$(p,x)^{48}$V	16.55 ± 2.09 mb	^{nat}Fe$(\pi^+,x)^{48}$V	16.25 ± 2.05 mb
^{nat}Fe$(p,x)^{51}$Cr	29.47 ± 11.61 mb	^{nat}Fe$(\pi^+,x)^{51}$Cr	28.19 ± 11.11 mb
^{nat}Fe$(p,x)^{52}$Fe	0.49 ± 0.07 mb	^{nat}Fe$(\pi^+,x)^{52}$Fe	0.54 ± 0.08 mb
^{nat}Fe$(p,x)^{52}$Mn	10.31 ± 1.16 mb	^{nat}Fe$(\pi^+,x)^{52}$Mn	10.48 ± 1.18 mb
^{nat}Fe$(p,x)^{54}$Mn	44.82 ± 8.83 mb	^{nat}Fe$(\pi^+,x)^{54}$Mn	43.21 ± 8.51 mb
^{nat}Fe$(p,x)^{55}$Co	0.62 ± 0.08 mb	^{nat}Fe$(\pi^+,x)^{55}$Co	0.51 ± 0.07 mb

the γ lines, the activated foils were counted twice: a short (10 minutes) measurement immediately after the irradiation and a longer one (about eight hours) later. The analysis was performed using the CANBERRA GENIE 2000 and the PROCOUNT 2000 software, which are comprehensive environments for data acquisition, display, and analysis. They include a set of spectrum analysis algorithms, which provide nuclide identification, interference correction, weighted mean activity, background subtraction, and efficiency correction. They also take into account geometrical effects, self-absorption in the sample, and decay of the isotope during the measurements, and provide a global uncertainty. Only the radioisotopes with an activity higher than $1Bq$ were considered for the cross-section calculations.

III. RESULTS

The beam effective cross section σ for each of the reactions of interest was derived from expression (1) by employing the values of N_x, ϕ', $A(t)$, t_{WAIT}, and t_{IRR}, obtained as explained in Sec. II. The cross sections of the proton- and pion-induced reactions were calculated from expressions (2) and (3). The foil exposed out of beam did not show any significant induced activity, confirming that the contribution of the scattered radiation (background) to the overall activity is negligible. Tables II and III list the cross sections of the spallation reactions that generated an activity in the foils higher than $1Bq$. The global uncertainty is the quadratic sum of the uncertainty on the γ spectrometry, the one on the IC calibration factor (10%) and the uncertainty on the foil thickness, i.e., on the knowledge of N_x. The uncertainty on the beam composition is not taken into account since it is below 2% [7]. The production of the radioisotopes listed in Tables II and III derives only from the proton- and pion-induced spallation reactions. For the reactions on $^{\mathrm{nat}}$Cu foils the cross section is the average of the values obtained from the three thicknesses.

A comparison between the cross section obtained at 120 GeV and the ones found in the literature at lower energies is given in the Appendix, which shows the data available for proton-induced spallation reactions (for the pion-induced reactions no data are available) at energies higher than 500 MeV.

IV. CONCLUSIONS

A comparison with literature data of the cross sections of proton- and pion-induced spallation reactions on $^{\mathrm{nat}}$Cu and $^{\mathrm{nat}}$Fe targets obtained in this experiment showed that in most cases the cross section at 120 GeV is comparable with the values available at the highest energies, i.e., around

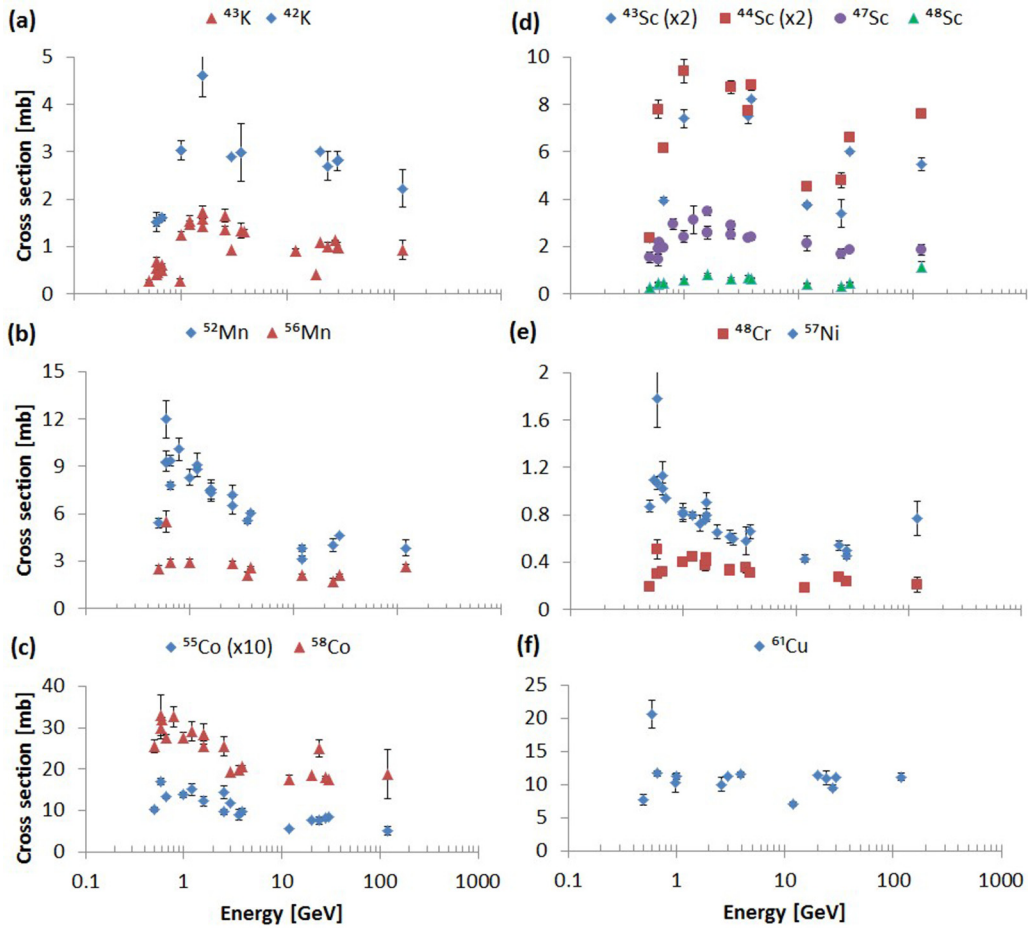

FIG. 2. (Color online) Cross sections of the spallation reactions on $^{\mathrm{nat}}$Cu for the production of: (a) potassium, (b) manganese, (c) cobalt, (d) scandium, (e) chromium, and (f) copper isotopes.

20–30 GeV, confirming that the cross section is energy independent above a certain energy. This behavior is coherent with the fact that above about a few hundred MeV, the total elastic and nonelastic cross sections for hadron-nucleus collisions are approximately constant [1]. This is foreseen by many physical models: the Sihver model [13], valid for $Z_{target} \leqslant 26$, which assumes that in a proton-nucleus interaction the cross section is energy independent for energies above 200 MeV; the limiting fragmentation model [14], which assumes the energy independence of the cross section for sufficiently high energies of the bombarding particle; the Letaw model [15], valid for $Z_{target} > 5$, which assumes that in a proton-nucleus interaction the cross section is energy independent above 2 GeV, with a possible small increase at very high energies ($\geq$100 GeV); the Glauber model [16], which allows us to compute reliably the hadron-nucleus cross section on the basis of the hadron-proton one and of the nuclear density distribution, which predicts cross sections almost constant at energies above a few GeV with a slow increase at the highest energies. Further activation experiments are foreseen in the future to validate the results presented in this paper.

ACKNOWLEDGMENTS

The authors wish to thank Matteo Magistris for providing access to the γ-spectrometry laboratory, Nicolas Riggaz and Biagio Zaffora for performing the γ-spectrometry measurements, and Clizia Severino for helping in some of the measurements.

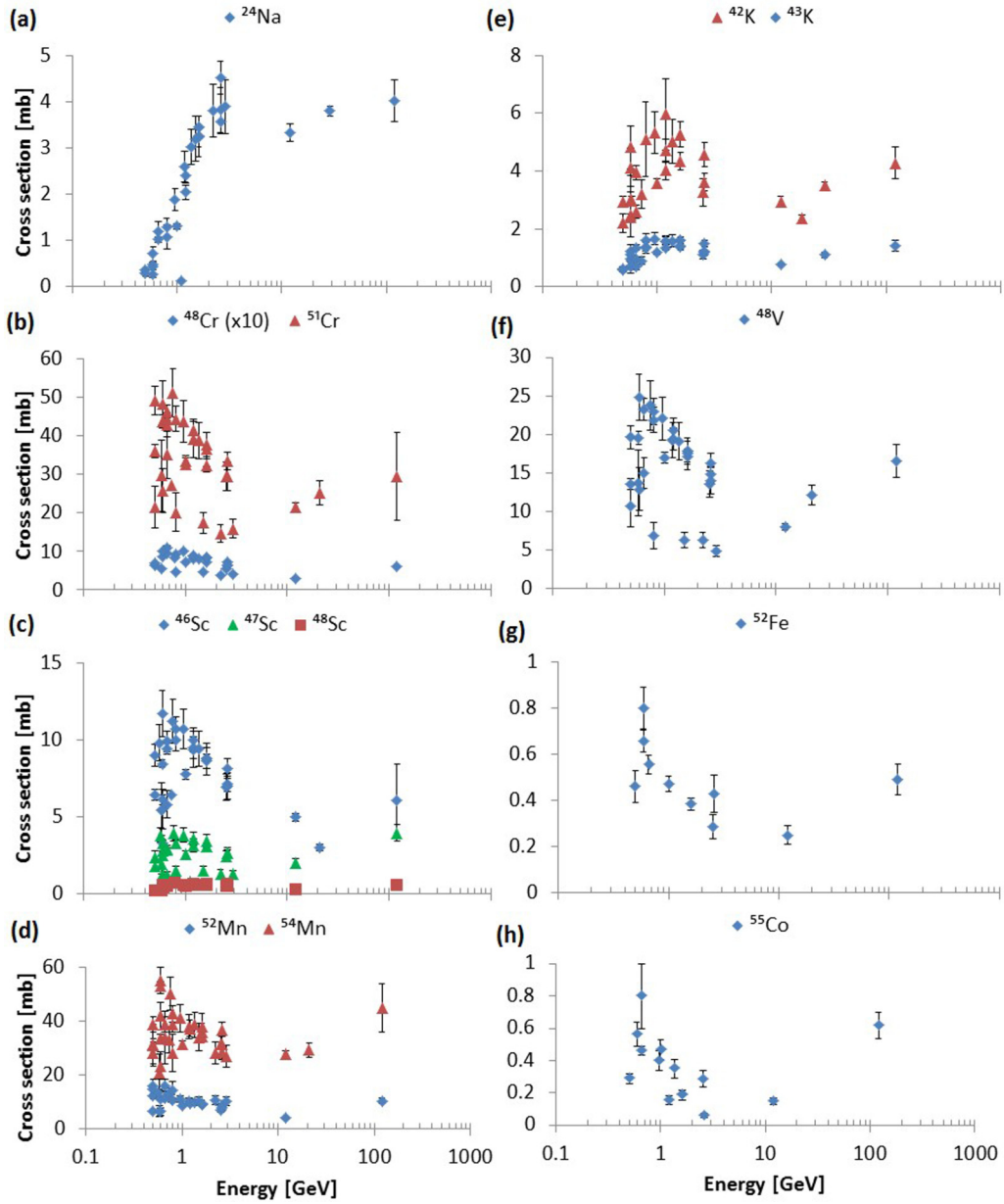

FIG. 3. (Color online) Cross sections of the spallation reactions on ^{nat}Fe for the production of: (a) sodium, (b) chromium, (c) scandium, (d) manganese, (e) potassium, (f) vanadium, (g) iron, and (h) cobalt isotopes.

APPENDIX

Figures 2 and 3 plot the cross-section values available in the literature [5] as a function of energy for proton-induced spallation reactions on ^{nat}Cu and ^{nat}Fe, respectively, at energies higher than 500 MeV, together with the values derived in this paper at 120 GeV. The cross-section distributions for reactions where very few data are available in the literature [^{nat}Cu$(p,x)^{41}$Ar, ^{nat}Fe$(p,x)^{41}$Ar, ^{nat}Fe$(p,x)^{43}$Sc, ^{nat}Fe$(p,x)^{44}$Sc] are not shown.

[1] D. Filges and F. Goldenbaum, *Handbook of Spallation Research* (Wiley-VCH, Weinheim, 2009).

[2] W. S. Charlton, T. A. Parish, A. P. Belian, and C. A. Beard, Nucl. Instrum. Meth. B **142**, 9 (1998).

[3] National Council on Radiation Protection and Measurements (NCRP), Report No. 144, 2005, doi:10.1093/rpd/nch479.

[4] L. Sihver, D. Mancusi, K. Niita, T. Sato, L. Townsend, C. Farmer, L. Pinsky, A. Ferrari, F. Cerutti, and I. Gomes, Acta Astronaut. **63**, 865 (2008).

[5] Nuclear reaction database (EXFOR), http://cdfe.sinp.msu.ru/ (2013).

[6] A. Mitaroff and M. Silari, Radiat. Prot. Dosim. **102**, 7 (2002).

[7] H. W. Atherton, C. Bovet, N. Doble, G. Von Holtey, L. Piemontese, A. Placci, M. Placidi, D. E. Plane, M. Reinharz, and E. Rossa, CERN Yellow Report 80-07 (1980).

[8] G. Battistoni, S. Muraro, P. R. Sala, F. Cerutti, A. Ferrari, S. Roesler, A. Fassò, and J. Ranft, in *Proceedings of the 2006 Hadronic Shower Simulation Workshop*, Fermilab, US, 2006, edited by M. Albrow and R. Raja, AIP Conference Proceeding 896, 31 (2007).

[9] A. Ferrari, P. R. Sala, A. Fassò, and J. Ranft, CERN-2005-10/INFN/TC_05/11, SLAC-R-773, 2005, http://www.slac.stanford.edu/cgi-wrap/getdoc/slac-r-773.pdf

[10] H. Crannell, C. J. Crannell, H. Whiteside, J. F. Ormes, and M. J. Ryan, Phys. Rev. D **7**, 730 (1973).

[11] A. Ferrari, F. P. La Torre, G. P. Manessi, F. Pozzi, and M. Silari [Phys. Rev. Special Topics Accel. Beams (to be published)].

[12] GoodFellow, see online catalog at http://www.goodfellow.com

[13] L. Sihver, C. H. Tsao, R. Silberberg, T. Kanai, and A. F. Barghouty, Phys. Rev. C **47**, 1225 (1993).

[14] J. Benecke, T. T. Chou, C. N. Yang, and E. Yen, Phys. Rev. **188**, 2159 (1969).

[15] J. R. Letaw, R. Siberberg, and C. H. Tsao, Astrophys. J. Suppl. Ser. **51**, 271 (1983).

[16] R. J. Glauber and G. Matthiae, Nucl. Phys. B **21**, 135 (1970).